

Theoretical study of electron structure of superheavy elements with an open $6d$ shell, Sg, Bh, Hs and Mt

B.G.C. Lackenby,¹ V.A. Dzuba,¹ and V.V. Flambaum^{1,2}

¹*School of Physics, University of New South Wales, Sydney 2052, Australia*

²*Johannes Gutenberg-Universität Mainz, 55099 Mainz, Germany*

We use recently developed efficient versions of the configuration interaction method to perform *ab initio* calculations of the spectra of superheavy elements seaborgium (Sg, $Z = 106$), bohrium (Bh, $Z = 107$), hassium (Hs, $Z = 108$) and meitnerium (Mt, $Z = 109$). We calculate energy levels, ionization potentials, isotope shifts and electric dipole transition amplitudes. Comparison with lighter analogs reveals significant differences caused by strong relativistic effects in superheavy elements. Very large spin-orbit interaction distinguishes subshells containing orbitals with a definite total electron angular momentum j . This effect replaces Hund's rule holding for lighter elements.

I. INTRODUCTION

Theoretical study of electron structure of superheavy elements (SHE, nuclear charge $Z > 103$) is an important area of research closing the gaps in relevant experimental data. While all SHE up to oganesson (Og, $Z = 118$) have been synthesized and named [1–3], experimental data on their spectra are absent.

The heaviest elements for which experimental spectroscopic data are available are nobelium (No, $Z = 102$) [4, 5] and lawrencium (Lr, $Z = 103$) [6]. Ionization potential (IP) has been measured for both atoms and the frequency of the strong $7s^2 \ ^1S_0 \rightarrow 7s7p \ ^1P_1^o$ electric dipole transition is measured for No. For heavier SHE the data come only from theory. There are many accurate calculations for atoms with relatively simple electronic structure, which includes atoms and ions with few electrons above closed shells (usually not more than four, see, e.g. Refs. [7–17]). This constitutes less than a half of the SHE in the range $104 \leq Z \leq 118$. Most of the SHE have an open $6d$ or $7p$ shell with more than four electrons. Till recently, the only available tool to perform calculations for such systems was the multi-configuration Dirac-Fock method (MCDF, see, e.g. review [18]). Some of the MCDF results we discuss in section VI. There are some model calculations of the basic parameters of the atoms, such as IP [19] and polarizabilities [20]. Accurate *ab initio* calculations of the spectra are practically absent. This is an unfortunate situation since from the study of relatively simple SHE we know that strong relativistic effects often bring significant difference in properties of SHE compared to their lighter analogs. Similar effects are expected for all SHE, including those with open shells. To address the problem, we have developed efficient versions of the configuration interaction (CI) approach, which allows study of atoms with any number of valence electrons. This includes the so-called CIPT method (configuration interaction with perturbation theory, [21]) and its fast version, the FCI method (fast configuration interaction [22]). Both methods are based on the idea that off-diagonal matrix elements between highly excited states can be neglected in the CI matrix. This allows one to reduce the problem to

a much smaller matrix with modified matrix elements. The methods were tested on such open-shell systems as Yb and No (including states with excitations from the $4f$ and $5f$ subshells) [21, 22], Ta [23], W and I [21], and superheavy elements Db [23] and Og [24]. Db is the first SHE with an open $6d$ shell that has been studied using the CIPT method [21, 25]. Its ground-state configuration is $[\text{Rn}]5f^{14}7s^25d^3$, i.e. it has five valence electrons above closed shells, which makes it difficult to use other methods. Lighter neighbours of Db, Rf (four valence electrons) and Lr (three valence electrons) were studied with the use of the powerful CI+all-order method [26, 27]. The use of the latter approach for Db is very problematic and is practically impossible for heavier elements. Following the successful use of the CIPT for Db, we apply it in the present work to heavier elements Sg, Bh, Hs and Mt ($106 \leq Z \leq 109$).

In this work we present the low-lying odd and even states of SHE $Z = 106$ – 109 including the allowed E1 transition amplitudes and rates from the ground state to odd parity states. We also calculate the ionization potential and isotope shift parameters for these elements.

The paper progresses as follows; in Section II we give a brief overview of the CIPT technique and how we implement it for the SHE. In Section III we discuss the accuracy of the calculations. In Section IV we give a brief discussion on the calculation of E1 transitions and corresponding isotope shift parameters between synthesized and predicted meta-stable SHE. In sections VA, VB, VC and VD we discuss the results of the CIPT on Sg I, Bh I, Hs I and Mt I atoms respectively. For reference we present the low-lying spectrum for Sg I and Bh I in Table III and Hs I and Mt I in Table IV and the E1 transitions and isotope shift parameters in Table V. In Section VI we present the ionization potentials of the four elements and compare them with other calculations.

II. CIPT METHOD

As mentioned above, an open $6d$ -shell with more than three valence electrons makes established many-

body methods too computationally expensive to be viable. This computational cost is reduced using a combination of configuration interaction (CI) and perturbation theory (PT) which was first introduced in [21] and used in [23, 24] for calculating the spectra of SHE Db ($Z = 105$) and Og ($Z = 118$). In this work we give a brief outline of the CIPT method and its implementation for the elements we calculate. For an in-depth discussion please refer to [21]. A fast version of this method has been developed in [22].

To generate the single-electron wavefunctions for all the elements, we use the V^{N_e-1} approximation (where N_e is the total number of electrons) [28, 29] where the Hartree-Fock calculations are performed for the singly-charged open-shell atom with a $6d^n 7s$ configuration, where $n = 4, 5, 6$ and 7 for Sg, Bh, Hs and Mt respectively. The single-electron basis states are calculated in the field of the frozen atomic core. The basis sets are generated using a B-spline technique [30] with 40 B-spline states in each partial wave of order 9 in a box with radius $40 a_B$ (where a_B is the Bohr radius) with partial waves up to $l_{max} = 4$ (where l is orbital angular momentum) and the many-electron basis states $|i\rangle = \Phi_i(r_1, \dots, r_{N_e})$ (where r_j is the radial position of the j th electron) for the CI calculations are formed by making all possible single and double excitations from reference low-lying non-relativistic configurations of the atom. This set of many-body electron wavefunctions is ordered from lowest to highest energy and divided into two sets,

- P : A small set of low energy wavefunctions ($i \leq N_{\text{Eff}}$, where N_{Eff} is the number of wavefunctions in the low energy set) that give dominant contributions to the CI wavefunction.
- Q : A large set of high energy wavefunctions ($N_{\text{Eff}} < i \leq N_{\text{total}}$) that are corrections to the wavefunctions from P .

The CI wavefunction is written as an expansion over single-determinant many-electron states $|i\rangle$ from these two sets,

$$|\Psi\rangle = \sum_{i=1}^{N_{\text{Eff}}} c_i |i\rangle + \sum_{i=N_{\text{Eff}}+1}^{N_{\text{total}}} c_i |i\rangle. \quad (1)$$

where c_i are coefficients of expansion. The CI Hamiltonian is truncated by neglecting the off-diagonal matrix elements of the CI Hamiltonian between terms in Q ($\langle i|H^{\text{CI}}|j\rangle = 0$ for $|i\rangle, |j\rangle \in Q$), which reduces the problem of finding the wave function and corresponding energy to a matrix eigenvalue problem of the size P with modified CI matrix

$$(H^{\text{CI}} - EI)X = 0, \quad (2)$$

where I is unit matrix, the vector $X = \{c_1, \dots, c_{N_{\text{eff}}}\}$ and the low energy matrix elements of H^{CI} are modified

to include perturbative contributions between states in P and Q .

$$\langle i|H^{\text{CI}}|j\rangle \rightarrow \langle i|H^{\text{CI}}|j\rangle + \sum_k \frac{\langle i|H^{\text{CI}}|k\rangle \langle k|H^{\text{CI}}|j\rangle}{E - E_k}. \quad (3)$$

where $|i\rangle, |j\rangle \in P$, $|k\rangle \in Q$, $E_k = \langle k|H^{\text{CI}}|k\rangle$, and E is the energy of the state of interest.

Both the Breit interaction (magnetic interaction and retardation)[31, 32] and quantum electrodynamic (QED) radiative corrections (Ueling potential and electric and magnetic form factors) [33] are included in the calculations as described in our earlier works (see, e.g. [16]). As both the Breit and QED radiative corrections scale with atomic charge, Z faster than the first power [16], their contribution to the energy levels of SHE is non-negligible. It was shown in [23] that the magnitude of the combined correction to the energy levels of Db is at most 200 cm^{-1} . A similar correction is expected for the SHE in this work.

For each level we calculate the Landé g -factor and compare it to the non-relativistic expression,

$$g_{\text{NR}} = 1 + \frac{J(J+1) - L(L+1) + S(S+1)}{2J(J+1)}. \quad (4)$$

Where possible, for each level we use g_{NR} to find an analogous state in the lighter element to obtain an approximate label in the LS coupling scheme. In fact, LS notations do not make sense for the highly relativistic SHE states due to very large spin-orbit interaction (so the eigenvectors will look strongly mixed in LS notation), we only use LS notations for comparison with lighter elements. Otherwise, we label the n th sequential state of total angular momentum J and parity by n_J^{parity} .

III. ESTIMATION OF THE ACCURACY

Theoretical uncertainty is dominated by incomplete treatment of inter-electron correlations. These correlations can be further separated into core-valence and valence-valence correlations. We will discuss each of these separately. For the SHE calculations, the core includes all states in closed shells from $1s$ to $5f$ containing one hundred electrons occupying one hundred states. All other states, including states of the $6d$ and $7s$ shells are treated as valence states. Only valence states are used in calculation of the CI matrix. This means that we neglect core-valence correlations. To estimate the corresponding uncertainties, we perform calculations of the energy levels of gold and roentgenium (Rg, $Z=111$). Both these elements have one external electron above a closed $5d$ or $6d$ shell. We perform the calculations using the correlation potential method [34, 35]. In this method, core-valence correlation corrections are obtained using the electron self-energy operator (correlation potential)

Table I. Removal energies (cm^{-1}) for states of external electron of Au and Rg calculated in different approximations. RHF is relativistic Hartree-Fock, $\Sigma(nd)$ are Brueckner orbital energies calculated with correlation potential Σ , in which summation over core states is limited to $5d$ or $6d$ shell only. $\Sigma(\text{all})$ are the energies calculated with full summation over core states.

	Au			Expt [37]
	RHF	$\Sigma(5d)$	$\Sigma(\text{all})$	
$6s_{1/2}$	60 179	75 539	77 878	74 409
$6p_{1/2}$	29 303	36 508	37 322	37 051
$6p_{3/2}$	26 664	32 314	32 785	33 324
$6d_{3/2}$	11 929	12 423	12 439	12 457
$6d_{5/2}$	11 875	12 344	12 357	12 376
	Rg			
	RHF	$\Sigma(6d)$	$\Sigma(\text{all})$	
$7s_{1/2}$	83 436	101 901	106 780	
$7p_{1/2}$	38 006	49 996	52 269	
$7p_{3/2}$	26 550	33 659	34 685	
$7d_{3/2}$	11 859	12 594	12 656	
$7d_{5/2}$	11 738	12 383	12 428	

Σ^1 calculated by summation of the diagrams in the many-body perturbation theory. The operator Σ is defined by the correlation correction to the energy of the valence electron on the orbital n , $\delta E_n = \langle n | \Sigma | n \rangle$. For the Au and Rg calculations, the upper complete d -shell ($5d$ or $6d$) is attributed to the core, and the correlation interaction of the external electron with the core is described by a correlation potential Σ .

Calculation of Σ involves a summation over all core states from $1s$ to $5d$ for Au or $6d$ for Rg. This summation is strongly dominated by the upper d -shell. E.g., the $5d$ shell gives about 90% of the correlation correction to the energies of the $6s$ and $6p$ valence states of Au, and more than 80% of the correlation correction to the energies of the $7s$ and $7p$ valence states of Rg (see Table I). This is because of the small energy interval between the energies of the $5d$ (or $6d$) state and the energies of lowest valence states. Since correlation correction to the energy of the s and p valence states is about 20%, the effect of neglecting inner-core contributions to the core-valence correlations is about 1 to 2% of the energy of valence states.

It is interesting to note that in the second order of many-body perturbation theory, the correlation potential Σ always overestimates the value of the correlation correction. This is because it does not include the

effect of screening of inter-electron interaction by other atomic electrons. This effect appears in higher orders of perturbation theory. Its proper inclusion leads to very accurate results (see, e.g. [34, 38]).

Since in the present work we do not go beyond the second order, we have the fortunate situation where neglecting inner-core contributions to Σ has a similar effect on its value as the screening would do. In other words, the effect of neglecting the higher-order perturbative contributions on the calculated energies partially compensates the effect of neglecting screening of interelectron interactions. The data in Table I show that this is the case at least for the $6s$ state of Au (and probably for the $7s$ state of Rg) where the correlation correction is the largest in value. Therefore, it is reasonable to assume that the theoretical uncertainty is dominated by valence-valence correlations. The main source for it is the perturbative treatment of the excited configurations. The best way of estimating the uncertainty is to compare the theoretical and experimental energies for lighter elements. We did this in detail for W [21], which is the lighter analog of Sg, and for pairs Ta and Db [23], and Rn and Og [39]. As follows from this comparison and from the analysis in Sections V A, V B, the theoretical uncertainty for the energies is on the level of $\sim 1000 \text{ cm}^{-1}$, sometimes a little higher (e.g. $\sim 2000 \text{ cm}^{-1}$ for odd states of Bh). The uncertainty for ionization potentials is on the level of a few percent (see section VI).

IV. ELECTRIC DIPOLE TRANSITIONS AND ISOTOPE SHIFTS

In the spectroscopic measurements, the frequencies of strong electric dipole (E1) optical transitions ($\omega < 40000 \text{ cm}^{-1}$) are likely to be measured first as it has been done for the $^1S_0 \rightarrow ^1P_1^o$ transition in No ($Z = 102$) [4]. Broad spectrum scans for strong lines are unfeasible and therefore *a priori* estimates of both a transition frequency and its strength from theoretical calculations will aid the experiments on SHE. Calculation of frequencies will be considered in section V. In this work we also calculate the E1 transition amplitudes and rates for the major optical transitions between the ground state and the lowest states of opposite parity (odd states) for each of the four SHE of interest. To calculate the E1 transition amplitude D_{E1} between two states $|a\rangle$ and $|b\rangle$, we use a self-consistent random-phase approximation (RPA) to simulate the atom in an external electromagnetic field. This results in an effective dipole field for the electrons that includes direct and exchange core polarization. An in-depth discussion of this method can be found in Ref. [40, 41]. The results in the RPA approximation are gauge-invariant [40]. However, when you calculate correlation corrections beyond RPA, the length form of the E1 operator usually gives better results for low-frequency transitions. Indeed, the calculation of the correlation corrections

¹ Do not confuse this with the QED self-energy operator which we included using the radiative potential method [33]. This is the many-body self-energy operator, which for example, has been defined in the textbook [36]. We calculate this operator using a Feynman diagram technique with relativistic Hartree-Fock Green's functions [34].

can be made explicitly gauge-invariant in the case of one electron above closed shells [35, 42]. However, in the velocity form some correlation corrections are proportional to $1/\omega$ and become very large for small frequencies ω [35, 42]. This is the reason why we prefer to perform all calculations using the length form of the E1 operator.

Note that comparison of results in different gauges is not always a good test of accuracy. For example, in the RPA approximation and in the correlation potential approach described in Ref. [35, 42], velocity and length forms give exactly the same results though the error is still finite. Therefore, to estimate the accuracy of the calculations we use comparison with available experimental data (see Table II).

The E1 transition rates, A_{E1} , are calculated using (in atomic units),

$$A_{E1} = \frac{4}{3} (\alpha\omega)^3 \frac{D_{E1}^2}{2J+1} \quad (5)$$

where J is the angular momentum of the upper state, α is the fine structure constant and ω is the frequency of the transitions in atomic units. All calculated amplitudes, D_{E1} , obey the selection rules for E1 transitions. The accuracy of these calculations cannot be tested directly due to the lack of experimental data on SHE and therefore we must rely on comparisons in lighter elements. Using the above method we calculated the E1 transition amplitudes and transition rates for the lighter analogs and compared them to available experimental data in Table II. The accuracy for the E1 amplitudes is $\sim 50\%$ which is sufficient to identify the strongest transitions. The calculated rates are *ab initio* using the amplitudes and energies calculated in the CIPT method.

Along with the excitation spectrum and E1 transitions we also calculate the isotope shift (IS) for each transition.

The IS is the difference in the transition frequency between two different isotopes. The IS is important for at least two reasons. First, it can be used to find the difference in nuclear radius between two isotopes. Second, it can be used to predict the spectra of heavier, meta-stable neutron rich isotopes from the spectra of short-lived, neutron deficient isotopes created and measured in the laboratory. These predictions can be compared to astronomical data [48–51] and could lead to the discovery of isotopes in the “island of stability” where it is expected that meta-stable, neutron-rich isotopes are created in cosmological events [52–55]. The IS of SHE is strongly dominated by the volume shift (also known as “field shift” in literature [56]), while the mass shift is negligible. Using CIPT, we calculate the excitation spectrum of the each isotope by varying the nuclear radius in the HF procedure described in the previous section. In the zero approximation only $s_{1/2}$ and $p_{1/2}$ electron waves penetrate the nucleus and for

these the dependence of IS on the nuclear radius R_N is $R_N^{2\gamma}$ where $\gamma = \sqrt{1 - (Z\alpha)^2}$ - see details in Ref. [57]. Higher waves undergo isotopic shifts due to change of the $s_{1/2}$ and $p_{1/2}$ wave functions and corresponding changes in the atomic Hartree-Fock potential - the core relaxation effect. Therefore, the dependence of the field IS on the nuclear radius in any atomic transition in multi-electron atoms is always $R_N^{2\gamma}$. Using the large-scale trend for nuclear radii $R_N \propto A^{1/3}$ the isotopic volume shift can be also approximated by $\delta\nu \propto A^{2\gamma/3}$ [48, 57] as nuclear shell fluctuations are suppressed [58]. The first form of the IS we present is given by

$$\delta\nu = E_2 - E_1 = a \left(A_2^{2\gamma/3} - A_1^{2\gamma/3} \right), \quad (6)$$

where A_1 and A_2 are atomic numbers for two isotopes ($A_2 > A_1$), E_1 and E_2 are the excitation energy for A_1 and A_2 respectively and a is a parameter which should be calculated for each transition. This form of the IS is convenient for non-neighbouring isotopes and predicting the spectra of meta-stable isotopes because there is a significant difference in the values of A for isotopes synthesized in laboratory and hypothetical meta-stable isotopes ($\Delta A \sim 10$). The $R_N \propto A^{1/3}$ trend is based on the constant nuclear density approximation due to finite range nuclear interactions. Variation of the nuclear shape and charge density may lead to significant deviations. Specific theoretical information about expected density distributions in SHE is presented in [59].

A more common form of isotope shift is the standard formula relating the change of atomic frequency to the change of nuclear charge radius

$$\delta\nu = F\delta \langle r^2 \rangle, \quad (7)$$

where the square of the nuclear charge radius is calculated using the Fermi distribution for the nuclear density. This formula (neglecting the mass shift) is convenient for extraction of the nuclear charge radius change from isotope shift measurements of nearby isotopes. Lastly, we introduce a new form of the IS which should be valid for all isotopes. Using the RMS (root mean squared) nuclear radius, $R_{rms} = \sqrt{\langle r^2 \rangle}$, and $\delta\nu \propto \delta R_{rms}^{2\gamma}$ [57] we can write the equation,

$$\delta\nu = \tilde{F} \frac{R_{rms,A_2}^{2\gamma} - R_{rms,A_1}^{2\gamma}}{\text{fm}^{2\gamma}} \quad (8)$$

where \tilde{F} is an IS parameter to be calculated for each transition.

V. CALCULATION OF ENERGY LEVELS, E1 TRANSITION RATES AND ISOTOPE SHIFT

Energy levels of SHE are calculated by solving the matrix eigenvalue problem (2) separately for states of given value of the total angular momentum J and parity. The

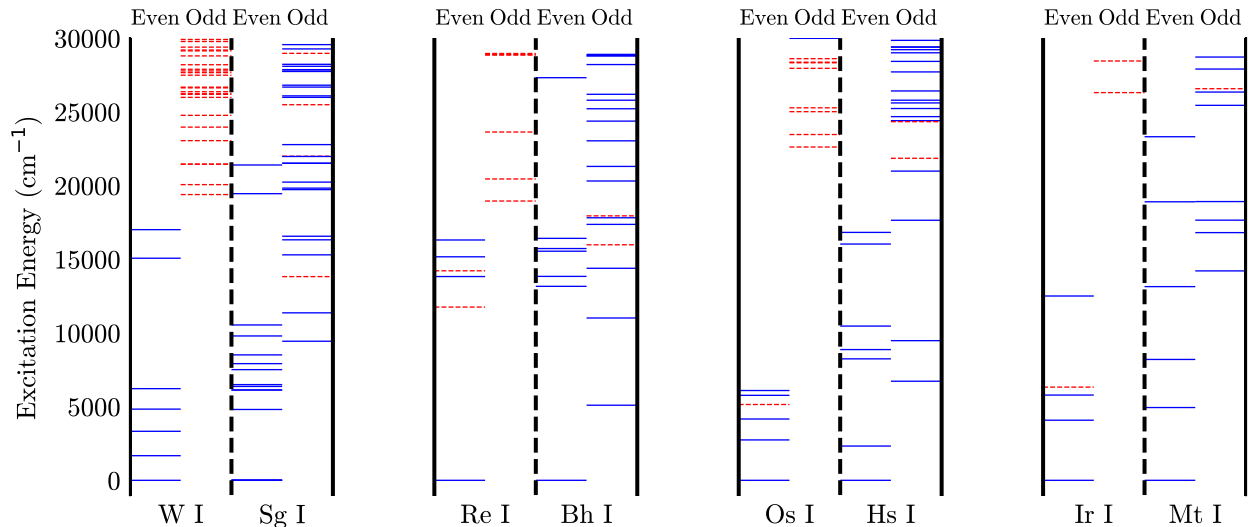


Figure 1. Comparison of low-energy excitations of SHE and their respective lighter analogs. For each element, the states are split between odd and even parities. The solid (blue) lines represent states with $6s^2$ or $7s^2$ in the electronic configuration for the lighter elements and SHE respectively. The dashed (red) lines are all other states where an s electron has been excited from the filled $6s$ or $7s$ shell. Experimental energies were used for W I, Bh I, Hs I and Ir I. [37]

specific details for each considered SHE are presented below. Most previous theoretical works on these SHE present the calculation of the first ionization potential, which we discuss in Section VI. Fig. 1 compares calculated spectra of low-lying states of SHE with experimental data on their lighter analogs. One can see a significant difference in the spectra of SHE and their lighter analogs, which is common for all considered atoms. Almost all low-lying odd states of lighter atoms correspond to the $6s - 6p$ excitation from the ground state. In contrast to that, in SHE the $7s$ state is significantly lower on the energy scale than the $6d$ state due to relativistic effects. Therefore, dominant excitations occur from the $6d$ state, i.e. low-lying odd states correspond to the $6d - 7p$ excitations from the ground state. Since the $6d - 7p$ energy interval is smaller than the $6s - 6p$ one, the density of odd states is higher for the SHE.

A. The Seaborgium Atom

Seaborgium was first experimentally detected in 1974 [60]. Since the initial discovery there has been continued interest and study into its physical and chemical properties including the discovery of isotopes with longer lifetimes. There exist some experimental results for Sg I in the field of chemistry [61]. However, there are no spectroscopic results available. The ground state configuration of Sg I is expected to be $[\text{Rn}]5f^{14}6d^47s^2$, similar to the ground state of its lighter homologue (W I, ground configuration: $[\text{Xe}]4f^{14}5d^46s^2$).

We calculated the first 6 even parity states and the ground state was found to be the $[\text{Rn}]5f^{14}6d^47s^2 \ ^5D_0$ state. To calculate the even states we use three reference configurations, $6d^47s^2$, $6d^57s$ and $6d^6$ to make states in the effective CI matrix (first terms in the expansion (1) and in the CI effective Hamiltonian (3)). All other states, which are treated as corrections to the states from reference configurations (second terms in the expansion (1) and in the CI Hamiltonian (3)) are obtained by exciting one or two electrons from the reference configurations. Similarly, for odd parity states we use the reference states from the $6d^47s7p$, $6d^37s^27p$ and $6d^57p$ configurations. All calculated even and odd energy levels are presented in Table III. Similar calculations were performed for W I using analogous reference states and the same parameters. Comparing these results to the experimental spectrum [37] we found a maximum discrepancy of $|\Delta| \approx 600 \text{ cm}^{-1}$ and expect a similar accuracy for our Sg I calculations. Note that this accuracy is slightly better than what was reported in Ref. [21] due to inclusion of a larger number of states into the effective CI matrix.

Comparing the spectrum of Sg I in Table III to the spectrum of W I [37], we can see the manifestation of relativistic effects. As discussed above, relativistic effects cause the $7s$ orbital in Sg I to be strongly contracted and more tightly bound in comparison to the $6s$ orbital in W I. The same effects also push out the $6d$ orbital of Sg I in comparison to the $5d$ orbital in W I. In the W I spectrum there are low-lying states corresponding to the $6s \rightarrow 5d$ excitation from the ground state (e.g., the $5d^56s \ ^7S_3$ state at $2\,951.29 \text{ cm}^{-1}$). In contrast, in

the Sg I spectrum, all low-lying even states belong to the $6d^47s^2$ configuration. The relativistic effects are more apparent in the low-lying odd parity states of Sg I. In W I all odd states correspond to the $6s \rightarrow 6p$ excitation from the ground state, while in Sg I most of the low-lying odd states correspond to the $6d \rightarrow 7p$ excitation. Only a few of the Sg I predicted in the optical region correspond to the $7s \rightarrow 7p$ excitation.

We calculate rates of electric dipole transitions from the ground state to excited states of the opposite parity using the approach described in Section IV. The results are presented in Table V. There are not many such transitions due to the zero value of the total angular momentum J in the ground state. Because of that, the transitions are only allowed to the odd states with $J = 1$. A few transitions are good candidates for the detection. The transition with the highest transition rate is $^5D_0 \rightarrow 9^1_1$ ($\omega = 40\,073\text{ cm}^{-1}$).

We also present the isotopic shift parameters, F and a from equations (6) and (7), in Table V for each respective E1 transition. The two isotopes we use are ^{269}Sg and ^{290}Sg ($R_{rms,269} = 5.8814\text{ fm}$ and $R_{rms,290} = 6.0145\text{ fm}$ respectively), where ^{290}Sg is the theoretically metastable ($N = 184$) isotope of Sg.

B. The Bohrium Atom

Bohrium was first discovered in 1981 [62]. No atomic spectra have been measured or calculated for any Bh isotopes or ions. When calculating the energy spectrum of Bh I, we use a similar approach as with Sg I. For the low-lying even parity spectrum we use an effective CI matrix build from the states of the $6d^57s^2$, $6d^67s$ and $6d^7$ reference configurations. For the odd parity spectrum we use the states from the $6d^57s7p$, $6d^47s^27p$ and $7d^67p$ reference configurations. The lowest six even parity states and low-lying odd parity states are presented in Table III. For an estimate of accuracy we calculated the low-lying spectrum of Re I (the lighter analogue of Bh) with similar parameters. Comparing the CIPT calculated spectrum to the experimental spectrum [37], the energy discrepancy (with respect to the ground state) was $\Delta \approx 900\text{ cm}^{-1}$ for the even parity states, while for the odd parity states $\Delta \approx 2000\text{ cm}^{-1}$.

The calculated Bh I ground state is $6d^57s^2\ ^6S_{5/2}$. As with Sg I, we see the relativistic effect of the tightly bound $7s$ electron which results in the primary excitation of the $6d$ electron. Comparing the spectrum of Bh I with that of Re I in Fig. 1 we see that there are several low-lying states in Re I corresponding to $6s \rightarrow 5d$ excitations (the lowest is at 11754.52 cm^{-1}), while there are no similar low-lying states in Bh I. The density of low-energy odd-parity states is much larger in Bh I than in Re I. The Bh I low odd-parity states are completely dominated by the $6d \rightarrow 7p$ excitations in calculated spectrum and there are no $7s \rightarrow 7p$ excitations. The

odd-parity state comparison between Bh I and Re I is similar to that of Sg I and W I in Section V A. In the spectrum of Re I [37] there do exist states corresponding to $5d \rightarrow 6p$ transitions from the ground state; however, they occur much higher in the spectrum compared to Bh I where the $6d \rightarrow 7p$ excitations dominate. It should be noted that the number of low-lying odd-parity states is larger in Bh I than in Re I. The lowest odd state of Bh I occurs at 12792 cm^{-1} , whereas in Re I the lowest odd state is at 18950 cm^{-1} .

Bh I has a large number of allowed low-energy optical E1 transitions from the ground state, which are presented in Table V. The isotope shift parameters, a and F , are calculated using formulas (6) and (7) after calculating the atomic spectra for the theoretically metastable isotope of ^{270}Bh using the CIPT method. We use the values of RMS nuclear radii $R_{rms,270} = 5.8879\text{ fm}$ for ^{291}Bh and $R_{rms,291} = 6.0207\text{ fm}$ for ^{291}Bh .

C. The Hassium atom

Hassium ($Z = 108$) was first synthesized in 1984 [63]. We present the low-lying levels and the first ionization energy of Hs I in Table IV. For the low-lying even spectrum effective CI reference states belong to the $6d^57s^2$, $6d^67s$ and $6d^7$ configurations. For the odd spectrum we use reference states of the $6d^57s7p$, $6d^47s^27p$ and $7d^67p$ configurations. Note that the half-filled $6d$ subshell makes computational methods particularly expensive. However, using the CIPT method the computation becomes tractable.

Once again it is interesting to compare the spectra of Hs I with the analogue Os I in the period above. In the even states of Os I there are states corresponding to the $6s \rightarrow 5d$ excitations from the ground state. In the Hs I spectrum all low-lying even states belong to the $6d^57s^2$ configuration. No states with the $7s \rightarrow 6d$ excitation were found. The odd states are similar to those of Sg and Bh, with the primary excitation $6d \rightarrow 7p$ in Hs I while there are no $5d \rightarrow 6s$ excitations in low Os I spectrum. The odd states of Hs I also lie much lower than those in Os I. The lowest odd state of Hs I is $13\,949\text{ cm}^{-1}$, while the first odd state of Os I occurs at $22\,615.69\text{ cm}^{-1}$ [37].

The allowed strong optical E1 transitions from the low-lying odd states to the ground state (5D_4) are presented in Table V. As with Bh I there is a large number of strong optical transitions. The transition with the largest rate is $3^0_2 \rightarrow ^5D_4$ ($\omega = 39\,268\text{ cm}^{-1}$). Other possibly detectable transitions include $5^0_3 \rightarrow ^5D_4$ ($\omega = 34\,812\text{ cm}^{-1}$) and $2^0_5 \rightarrow ^5D_4$ ($\omega = 34\,739\text{ cm}^{-1}$).

We also present the isotopic shift parameters for the Hs E1 optical transitions in Table V. These were calculated from the theoretical spectra (calculated with the CIPT method) with isotopes ^{270}Hs and ^{292}Hs with RMS nuclear radii $R_{rms,270} = 5.8879\text{ fm}$ for ^{292}Hs and $R_{rms,292} = 6.0207\text{ fm}$ for ^{270}Hs .

D. The Meitnerium Atom

Meitnerium ($Z = 109$) was first synthesized in 1982 [64]. The ground state of Mt 1 is expected to follow that of the element in the above period (Ir) with $[\text{Rn}]5f^{14}6d^77s^2\ ^4F_{9/2}$ which we confirm in the calculated spectrum presented in Table IV.

We use the same method as for previous elements to calculate the low-lying spectrum of Mt 1. We present the lowest six even states using the $6d^77s^2$, $6d^8, 7s$ and $6d^9$ reference configurations. We also present the first 12 odd parity states for which the $6d^77s7p$, $6d^67s^27p$ and $6d^87p$ configurations were used. The results are in Table IV. Comparison with lighter analog Ir 1 shows similar trend as for other SHE Sg, Bh and Hs.

We also present the allowed E1 transitions for Mt and the respective isotope shift parameters in Table V. The high energy of the odd states in Mt 1 result in a small number of allowed E1 transitions within optical region from the ground state compared to Bh and Hs. Promising transitions for future measurement include $^6F_{11/2}^\circ \rightarrow ^4F_{9/2}$ ($\omega = 38\,027\text{ cm}^{-1}$) and $^6D_{9/2}^\circ \rightarrow ^4F_{9/2}$ ($\omega = 33\,505\text{ cm}^{-1}$). All other rates are two or more orders of magnitude smaller. For the synthesized and metastable isotopes we use the RMS nuclear radii values, $R_{rms,276} = 5.9265\text{ fm}$ and $R_{rms,293} = 6.0330\text{ fm}$.

VI. IONIZATION POTENTIALS AND COMPARISON WITH OTHER DATA.

As well as calculating the spectrum of neutral Sg, Bh, Hs and Mt we also calculated their first ionization potentials (IPs). To calculate the IP for each atom we use the same single-electron basis set for a neutral atom and an ion. The ionization potential is found as a difference between ground state energies of the atom and its ion. The effective CI matrix was built from all states of the $6d^n7s$, $6d^{n-1}7s^2$ and $6d^{n+1}$ reference configurations ($n = 4-7$ for Sg through to Mt). States that were treated perturbatively were obtained by exciting one or two electrons from the reference configurations and generating all single-determinant states from these configurations. We start from calculating the IPs of lighter analogs of the SHE to compare them with experiment. The results are in Table VI. We also include in the table the results of the multi-configuration Dirac-Fock (MCDF) calculation [65, 66]. We do this because similar MCDF calculations have been used for the SHE (see Tables VII and VIII). The CIPT values of the IPs agree with experiment within few percent (error $<1\%$ for Ta, W, and Re, and $\sim 3\%$ for Os and Ir). We expect similar accuracy for the first IPs of SHE analogs presented in Table VIII. For comparison, the difference between MCDF values of IPs of W, Re and Os and experimental IPs is larger than 10% (Table VI).

Table VII shows some resonance (corresponding to

strong electric dipole transitions from the ground state) excitation energies for SHE and their lighter analogs calculated in the present work and by the MCDF method [65, 66]. The energies for lighter elements are compared to experiment. Our values are taken from Tables III and IV; for the MCDF energies we present all results which can be found in [65, 66]. There is a significant difference in the excitation energies of SHE, while for lighter atoms the difference is not so large. There is a $\sim 10\%$ difference from experiment in both calculations. There are too little data on the MCDF calculations to come to any conclusion about the reasons for the differences.

Finally, Table VIII shows IPs of SHE and their ions. We included the result of our previous work on Db [23] together with the relativistic Hartree-Fock (RHF) calculations which include semi empirical core-polarisation correction [20] and the MCDF results [65, 66]. There are two sets of MCDF results. One, in the column marked as MCDF, is what directly comes from the MCDF calculations. We also presented prediction of MCDF IPs corrected by extrapolation of the difference with experiment from lighter atoms (marked as ‘‘Extrap.’’). As one can see from Table VI the MCDF method tends to underestimate IPs by about 10%. Therefore, multiplying the calculated IPs by a factor ~ 1.1 extrapolated from lighter elements leads to better prediction of the IPs for SHE. Indeed, the extrapolated values are in better agreement with our CIPT calculations. Note however that the extrapolation assumes similarities between involved elements. In fact, they are significantly different. Ionization of lighter elements goes via removal of the s electron ($6s$ electron for W, Re and Os). In contrast, ionization of SHE goes via removal of the $6d$ electron. RHF calculations (see Ref. [20] and Table VIII) used a different type of extrapolation. Instead of extrapolating a final number, a term in the Hamiltonian was extrapolated. A term, simulating the effect of core polarisation, was added to the RHF Hamiltonian in Ref. [20]. Its strength was chosen to fit IPs of lighter atoms. Then the same term was used for SHE.

Studying IPs of SHE with open $6d$ -shell shows a significant difference in trends compared to their lighter analogs. These differences are convenient to discuss by looking at the diagram in Fig. 2. The diagram shows trends in IPs of SHE with open $6d$ -shell from Db to Mt together with the trends for lighter atoms from Ta to Ir. IPs for doubly ionized ions of lighter elements are also shown because they do not have external s -electrons, and further ionization of these ions goes via removal of a d -electron similar to what takes place for SHE.

First, we note that the change of IPs from Ta to Ir is smooth and almost monotonic, apart from a small local minimum at Re atom. It shows increasing of IP towards the fully filled $5d$ shell. The ionization occurs via removal of a $6s$ electron. The $6s$ orbital is not very sensitive to the details of energy structure of other shells, which explains the smooth behaviour of the IP trend.

In contrast, ionization of the SHE occurs via removal of a $6d$ electron. Strong relativistic effects manifest themselves in the trend of the IP change. A local maximum of the IP occurs for Sg atom that has four $6d$ electrons in the fully occupied $6d_{3/2}^4$ subshell. Removing an electron from a closed shell is difficult, therefore there is a local maximum. The next atom, Bh, has one more $6d$ electron, which has to occupy the $6d_{5/2}$ state. Due to large relativistic effects in SHE, there is a large fine structure interval between the $6d_{3/2}$ and $6d_{5/2}$ states and therefore a significantly smaller IP for Bh (see Fig. 2 and Table VIII). A similar effect is known for an open p shell where it is more pronounced. E.g., the IP of Bi, which has three $6p$ electrons, is smaller than for Pb, which has two $6p$ electrons corresponding to the closed $6p_{1/2}^2$ subshell. The effect is much more pronounced for SHE with an open $7p$ shell [16]. The IP of Mc ($Z=115$), which has three $7p$ electrons, is about 1.5 times smaller than the IP of Fl ($Z=114$), which has two $7p$ electrons.

To see whether a similar effect can be found in lighter atoms, we studied IPs of doubly ionized ions with an open d -shell (from $3d$ to $5d$). The ions were chosen because they do not have external s -electrons, and further ionization goes via removal of a d -electron. The results are shown in Fig. 2. Most IP values are taken from the NIST database [37]. However, NIST data for ions from Ta III to Ir III have poor accuracy. Therefore, we recalculated the IPs using the CIPT method. IPs of these ions show a different trend compared to the SHE. The maximum binding energy and hence the maximum IP is for a half filled d -shell in agreement with the non-relativistic Hund rule, which states that the maximum energy corresponds to the maximum possible value of the total spin. This holds even for the heaviest of the three groups of ions. Thus, the SHE elements with the open $6d$ shell represents the only known example of a strong manifestation of relativistic effects, making the energy difference between the $6d_{3/2}$ and $6d_{5/2}$ states more important than Hund's rule.

A similar manifestation of relativistic effects can be found in the trends of further ionization of the SHE ions (see Table VIII). In many cases (e.g., the Bh and Hs ions) ionization from the $6d$ shell stops as soon as the fully filled $6d_{3/2}^4$ subshell is reached. Further ionization occurs from the $7s$ subshell.

VII. CONCLUSION

Calculation of atomic spectra and optical E1 transitions for the elements in the superheavy region with open d -shells is novel. In spite of the extreme computational cost of existing methods, using perturbation theory we can calculate the low-lying energy states and relevant E1 transitions with a modest computational cost and with a small loss in accuracy [21]. In this work we presented the low-lying energy states for Sg I, Bh I, Hs I and Mt I including the optical transitions between

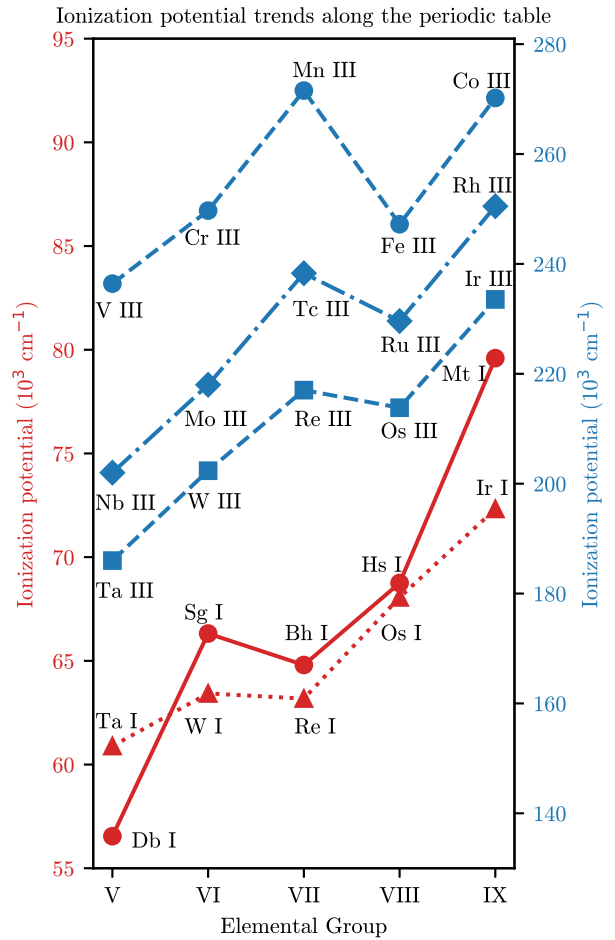


Figure 2. Plot of ionization trends for open d -shell elements. The IP trend lines for the doubly ionized elements (blue) use the scale on the right and the neutral IP trend lines (red) use the left. The IPs of neutral SHEs and the doubly ionized lighter homologues Ta III, W III, Re III, Os III and Ir III were calculated using the CIPT method. All other IPs are from Ref. [37].

the ground state and states of the opposite parity and their ionization potentials. For all SHEs we observed the relativistic effects, which contract the spectrum compared to their lighter analogs. This is advantageous as it results in a large number of states in the allowed E1 optical region and therefore enhances the likelihood of future measurements. These calculations will help to facilitate future experimental measurements of atomic spectra of these elements. We also presented the relevant isotopic field shift for optical E1 transitions for all four considered SHE. This may help the interpretation of future measurements and contribute to our understanding of the nuclear properties of elements in the superheavy region and potentially identify the existence of meta-stable superheavy isotopes in astronomical spectra.

-
- [1] P. J. Karol, R. C. Barber, B. M. Sherrill, E. Vardaci, and T. Yamazaki, *Pure App. Chem* **88**, 155 (2016).
- [2] J. H. Hamilton, S. Hofmann, and Y. T. Oganessian, *Annu. Rev. Nucl. Part. Sci.* **63**, 383 (2013).
- [3] Y. T. Oganessian, V. K. Utyonkov, Y. V. Lobanov, F. S. Abdullin, and A. N. Polyakov, *Nucl. Phys. A* **734**, 109 (2004).
- [4] M. Laatiaoui, W. Lauth, H. Backe, M. Block, and D. Ackermann, *Nature* **538**, 495 (2016).
- [5] P. Chhetri, D. Ackermann, H. Backe, M. Block, B. Cheal, C. Droese, C. E. Dullmann, J. Even, R. Ferrer, F. Giacoppo, S. Gotz, F. P. Hessberger, M. Huyse, O. Kaleja, J. Khuyagbaatar, P. Kunz, M. Laatiaoui, F. Lautenschlager, W. Lauth, N. Lecesne, L. Lens, E. MinayaRamirez, A. K. Mistry, S. Raeder, P. VanDuppen, T. Walther, A. Yakushev, and Z. Zhang, *Phys. Rev. Lett* **120**, 263003 (2018).
- [6] T. K. Sato, M. Asai, A. Borschevsky, T. Stora, N. Sato, Y. Kaneya, and K. Tsukada, *Nature* **520**, 209 (2015).
- [7] E. Eliav, S. Fritzsche, and U. Kaldor, *Nucl. Phys. A* **944**, 518 (2015).
- [8] V. Pershina, *Nucl. Phys. A* **944**, 578 (2015).
- [9] E. Eliav, U. Kaldor, Y. Ishikawa, M. Seth, and P. Pyykkö, *Phys. Rev. A* **53**, 3926 (1996).
- [10] V. Pershina, A. Borschevsky, E. Eliav, and U. Kaldor, *J. Phys. Chem. A* **112**, 13712 (2008).
- [11] Y. J. Yu, C. Z. Dong, J. G. Li, and B. Fricke, *J. Chem. Phys.* **128**, 124316 (2008).
- [12] A. V. Zaitsevskii, C. van Wüllen, and A. V. Titov, *Russ. Chem. Rev.* **78**, 1173 (2009).
- [13] C. Thierfelder, B. Assadollahzadeh, P. Schwerdtfeger, S. Schafer, and R. Schafer, *Phys. Rev. A* **78**, 052506 (2008).
- [14] A. Landau, E. Eliav, Y. Ishikawa, and U. Kaldor, *J. Chem. Phys.* **114**, 2977 (2001).
- [15] A. Borschevsky, L. F. Pasteka, V. Pershina, E. Eliav, and U. Kaldor, *Phys. Rev. A* **91**, 020501(R) (2015).
- [16] V. A. Dzuba and V. V. Flambaum, *Hyperfine Interactions* **237**, 160 (2016).
- [17] T. H. Dinh and V. A. Dzuba, *Phys. Rev. A* **94**, 052501 (2016).
- [18] C. Froese Fischer, M. Godefroid, T. Brage, P. Jönsson, and G. Gaigalas, *J. Phys. B* **49**, 182004 (2016).
- [19] A. Borschevsky, L. F. Pasteka, V. Pershina, E. Eliav, and U. Kaldor, *Phys. Rev. A* **91**, 020501(R) (2015).
- [20] V. A. Dzuba, *Phys. Rev. A* **93**, 032519 (2016).
- [21] V. A. Dzuba, J. C. Berengut, C. Harabati, and V. V. Flambaum, *Phys. Rev. A* **95**, 012503 (2017).
- [22] V. A. Dzuba, V. V. Flambaum, and M. G. Kozlov, *Phys. Rev. A* **99**, 032501 (2019).
- [23] B. G. C. Lackenby, V. A. Dzuba, and V. V. Flambaum, *Phys. Rev. A* **98**, 022518 (2018).
- [24] B. G. C. Lackenby, V. A. Dzuba, and V. V. Flambaum, *Phys. Rev. A* **98**, 042512 (2018).
- [25] A. J. Geddes, D. A. Czapski, E. V. Kahl, and J. C. Berengut, *Phys. Rev. A* **98**, 042508 (2018).
- [26] V. A. Dzuba, M. S. Safronova, and U. I. Safronova, *Phys. Rev. A* **90**, 012504 (2014).
- [27] V. A. Dzuba, M. S. Safronova, U. I. Safronova, and A. Kramida, *Phys. Rev. A* **94**, 042503 (2016).
- [28] H. P. Kelly, *Phys. Rev* **136**, 3B (1964).
- [29] V. A. Dzuba, *Phys. Rev. A* **71**, 032512 (2005).
- [30] W. R. Johnson, S. A. Blundell, and J. Sapirstein, *Phys. Rev. A* **37**, 307 (1988).
- [31] G. Breit, *Phys. Rev.* **34**, 4 (1929).
- [32] J. B. Mann and W. R. Johnson, *Phys. Rev. A* **4**, 1 (1971).
- [33] V. V. Flambaum and J. S. M. Ginges, *Phys. Rev. A* **72**, 052115 (2005).
- [34] V. A. Dzuba, V. V. Flambaum, P. G. Silvestrov, and O. P. Sushkov, *Phys. Lett. A* **131**, 461 (1988).
- [35] V. A. Dzuba, V. V. Flambaum, P. G. Silvestrov, and O. P. Sushkov, *J. Phys. B* **20**, 1399 (1987).
- [36] E. M. Lifshitz and L. P. Pitaevskii, *Statistical Physics Part 2*, 3rd ed. (Pergamon Press, 1980).
- [37] A. Kramida, Yu. Ralchenko, J. Reader, and NIST ASD Team, NIST Atomic Spectra Database (ver. 5.6.1), [Online]. Available: <https://physics.nist.gov/asd> [2019, March 18]. National Institute of Standards and Technology, Gaithersburg, MD. (2018).
- [38] V. A. Dzuba and V. V. Flambaum, *Phys. Rev. A* **77**, 012514 (2008).
- [39] B. G. C. Lackenby, V. A. Dzuba, and V. V. Flambaum, *Phys. Rev. A* **98**, 042512 (2018).
- [40] V. A. Dzuba, V. V. Flambaum, P. G. Silvestrov, and O. P. Sushkov, *Phys. Lett. A* **118**, 177 (1986).
- [41] V. A. Dzuba, V. V. Flambaum, and S. Schiller, *Phys. Rev. A* **98**, 022501 (2018).
- [42] V. A. Dzuba, V. V. Flambaum, P. G. Silvestrov, and O. P. Sushkov, *J. Phys. B* **20**, 3297 (1987).
- [43] M. Ortiz and R. Mayo-García, *J. Phys. B* **45**, 055701 (2012).
- [44] R. Kling and M. Kock, *J. Quant. Spec. Rad. Trans.* **62**, 129 (1999).
- [45] S. Ivarsson, J. Andersen, B. Nordström, X. Dai, S. Johansson, H. Lundberg, H. Nilsson, V. Hill, M. Lundqvist, and J. F. Wyart, *Astron. Astrophys.* **409**, 1141 (2003).
- [46] M. Kwiatkowski, P. Zimmermann, E. Biémont, and N. Grevesse, *Astron. Astrophys.* **135**, 59 (1984).
- [47] J. R. Fuhr and W. L. Wiese, *NIST Atomic Transition Probability Tables*, 77th ed. (CRC Press, Inc. Boca Raton, FL, 1996).
- [48] V. A. Dzuba, V. V. Flambaum, and J. K. Webb, *Phys. Rev. A* **95**, 062515 (2017).
- [49] N. G. Polukhina, *Phys.-Usp.* **55**, 614 (2012).
- [50] V. F. Gopka, A. V. Yushchenko, V. A. Yushchenko, I. V. Panov, and C. Kim, *Kinematics Phys. Celestial Bodies* **24**, 89 (2008).
- [51] V. Fivet, P. Quinet, E. Biémont, A. Jorissen, A. V. Yushchenko, and S. Van Eck, *Mom. Not. R. Astron. Soc.* **380**, 781 (2007).
- [52] S. Goriely, A. Bauswein, and H.-T. Janka, *Astrophys. J. Lett.* **738**, L32 (2017).
- [53] G. M. Fuller, A. Kusenko, and V. Takhistov, *Phys. Rev. Lett.* **119**, 061101 (2017).
- [54] A. Frebel and T. C. Beers, *Phys. Today* **71**, 30 (2018).
- [55] B. Schuettrumpf, M. A. Klatt, K. Iida, G. E. Schröder-Turk, J. A. Maruhn, K. Mecke, and P.-G. Reinhard, *Phys. Rev. C* **91**, 025801 (2015).
- [56] D. N. Stacey, *Rep. Prog. Phys.* **29**, 171 (1966).
- [57] V. V. Flambaum, A. J. Geddes, and A. V. Viatkina, *Phys. Rev. A* **97**, 032510 (2018).

- [58] I. Angeli and K. P. Marinova, *Atom. Data Nucl. Data Tabl.* **99**, 69 (2013).
- [59] W. Nazarewicz, *Nat. Phys.* **14**, 537 (2018).
- [60] A. Ghiorso, J. M. Nitschke, J. R. Alonso, C. T. Alonso, M. Nurmia, G. T. Seaborg, E. K. Hulet, and R. W. Lougheed, *Phys. Rev. Lett.* **33**, 1490 (1974).
- [61] B. M. Schädel, *Atomic Energy*, Vol. 604 (2012) pp. 579–604.
- [62] G. Münzenberg, S. Hofmann, F. P. Hessberger, W. Reisdorf, K. H. Schmidt, and J. H. R. Schneider, *Z. Phys* **A300**, 107 (1981).
- [63] G. Münzenberg, P. Armbruster, H. Folger, F. P. Hessberger, S. Hofmann, J. Keller, K. Poppenseiker, W. Reisdorf, K. H. Schmidt, H. J. Schoett, M. E. Leino, and R. Hingmann, *Z. Phys* **A317**, 235 (1984).
- [64] G. Münzenberg, P. Armbruster, F. P. Hessberger, S. Hofmann, K. Poppenseiker, W. Reisdorf, J. H. R. Schneider, W. F. W. Schneider, K. H. Schmidt, C. C. Sahm, and D. Vermeulen, *Z. Phys* **A309**, 89 (1982).
- [65] E. Johnson, V. Pershina, and B. Fricke, *J. Phys. Chem. A* **103**, 8458 (1999).
- [66] E. Johnson, B. Fricke, T. Jacob, C. Z. Dong, S. Fritzsche, and V. Pershina, *J. Chem. Phys.* **116**, 1862 (2002).

Table II. Comparison of E1 transition amplitudes and rates between experimental and CIPT values for the lighter analogs of SHE, W I, Re I, Os I, and Ir I. Here D_{E1} , A_{E1} and gf are the transition amplitude, rate and oscillator strength respectively. The experimental E1 amplitudes were calculated using the experimental energies, transition rates from experimental sources and Eq. (5). To calculate oscillator strengths for comparison with Re I transitions from Ref. [43], we use the formula $gf = 3.062 \times 10^{-6} \omega D_{E1}^2$ where ω is in cm^{-1} and D_{E1} is in (a.u.).

State	Expt.			CIPT		
	E^a (cm^{-1})	D_{E1} (a.u.)	A_{E1} ($\times 10^6 \text{ s}^{-1}$)	E (cm^{-1})	D_{E1} (a.u.)	A_{E1} ($\times 10^6 \text{ s}^{-1}$)
			W I			
13_1°	39 183.19	2.09(9)	178(15) ^b	39 606	3.07	400
			Os I			
4_4°	32 684.61	2.00(7)	31.53(221) ^c	32 576	2.36	43
3_4°	30 591.45	0.96	5.8 ^d	30 359	1.37	12
2_5°	30 279.95	1.40(5)	10.05(70) ^e	31 904	2.15	28
			Ir I			
$3_{11/2}^\circ$	39 940.37	1.72(22)	32(8) ^e	41 083	1.49	26
$4_{9/2}^\circ$	37 871.69	2.07(26)	47(12) ^e	39 227	1.52	28
$4_{7/2}^\circ$	37 515.32	1.73(22)	40(10) ^e	40 106	1.55	39
$6_{9/2}^\circ$	35 080.70	1.59(20)	22(6) ^e	36 703	2.72	74
$6_{11/2}^\circ$	34 180.46	1.45(7)	14.2(14) ^e	36 358	1.51	18
State	E^a (cm^{-1})	D_{E1} (a.u.)	gf	E (cm^{-1})	D_{E1} (a.u.)	gf
			Re I			
$6_{3/2}^\circ$	28 961.55	1.22(17)	0.132(36) ^f	29 303	1.80	0.29
$6_{7/2}^\circ$	28 889.72	2.26(27)	0.45(11) ^f	29 247	3.32	0.98
$6_{5/2}^\circ$	28 854.18	1.70(19)	0.254(56) ^f	29 505	2.51	0.57

^a Ref. [37], ^b Ref. [44], ^c Ref. [45], ^d Ref. [46], ^e Ref. [47], ^f Ref. [43]

Table III. Low-energy spectrum of even- and odd-parity states for Sg I, Bh I. We present the energy and Landé g -factor for each state J^{parity} . We present LS - notations only for comparison with lighter analogs. For SHE states where an analogous state cannot be found in the lighter analog the term is labeled according to the sequential number of the state (n) for the given J^{parity} group, n_J^{parity} .

Sg I				Bh I			
Major Configuration	Term	Energy (cm ⁻¹)	Landé g -factor	Major Configuration	Term	Energy (cm ⁻¹)	Landé g -factor
Even parity states							
(1) $6d^47s^2$	5D_0	0	0.00	$6d^57s^2$	$^6S_{5/2}$	0	1.78
(2) $6d^47s^2$	5D_1	4 834	1.50	$6d^57s^2$	$^4P_{3/2}$	13 062	1.32
(3) $6d^47s^2$	5D_2	7 614	1.44	$6d^57s^2$	$^4G_{7/2}$	13 828	1.15
(4) $6d^47s^2$	5D_3	9 607	1.39	$6d^57s^2$	$^4G_{11/2}$	14 981	1.19
(5) $6d^47s^2$	5D_4	10 335	1.27	$6d^57s^2$	$^4P_{1/2}$	15 659	1.90
(6) $6d^47s^2$	52P_0	13 592	0.00	$6d^57s^2$	$^4G_{9/2}$	16 447	1.17
Odd parity states							
(7) $6d^37s^27p$	1°_2	14 717	0.57	$6d^47s^27p$	$2^{\circ}S_{1/2}$	12 792	0.72
(8) $6d^37s^27p$	1°_1	17 043	0.71	$6d^47s^27p$	$6^{\circ}D_{1/2}$	17 781	1.66
(9) $6d^37s^27p$	2°_2	20 444	1.13	$6d^47s^27p$	$6^{\circ}D_{3/2}$	19 483	1.09
(10) $6d^37s^27p$	1°_3	20 628	0.97	$6d^57s7p$	$8^{\circ}P_{5/2}$	22 228	2.08
(11) $6d^47s7p$	$7^{\circ}F_0^{\circ}$	20 979	0.00	$6d^47s^27p$	$6^{\circ}P_{3/2}^{\circ}$	22 533	1.74
(12) $6d^37s^27p$	2°_1	22 041	2.02	$6d^47s^27p$	$6^{\circ}D_{5/2}^{\circ}$	22 930	1.26
(13) $6d^37s^27p$	1°_4	24 132	1.11	$6d^57s7p$	$8^{\circ}P_{7/2}^{\circ}$	24 020	1.67
(14) $6d^37s^27p$	3°_1	24 382	1.19	$6d^47s^27p$	$6^{\circ}D_{7/2}^{\circ}$	25 171	1.28
(15) $6d^47s7p$	$1^{\circ}S_0^{\circ}$	25 362	0.00	$6d^47s^27p$	$6^{\circ}D_{9/2}^{\circ}$	26 587	1.21
(16) $6d^37s^27p$	2°_3	25 966	1.29	$6d^47s^27p$	$6^{\circ}F_{5/2}^{\circ}$	28 060	1.57
(17) $6d^37s^27p$	1°_5	26 271	1.17	$6d^47s^27p$	$3^{\circ}_{1/2}$	29 823	0.44
(18) $6d^37s^27p$	3°_2	26 420	1.22	$6d^47s^27p$	$3^{\circ}_{3/2}$	29 885	1.55
(19) $6d^47s7p$	$7^{\circ}F_1^{\circ}$	27 030	1.40	$6d^47s^27p$	$3^{\circ}_{7/2}$	31 078	1.24
(20) $6d^37s^27p$	4°_2	27 416	1.74	$6d^47s^27p$	$4^{\circ}_{5/2}$	31 253	1.30
(21) $6d^47s7p$	$7^{\circ}F_2^{\circ}$	29 976	1.41	$6d^47s^27p$	$4^{\circ}_{7/2}$	32 814	1.37
(22) $6d^37s^27p$	3°_0	30 055	0.00	$6d^47s^27p$	$4^{\circ}_{3/2}$	33 459	1.40
(23) $6d^37s^27p$	2°_4	30 372	1.25	$6d^47s^27p$	$2^{\circ}_{9/2}$	33 575	1.06
(24) $6d^37s^27p$	3°_3	30 753	1.09	$6d^47s^27p$	$5^{\circ}_{5/2}$	33 738	1.04
(25) $6d^37s^27p$	5°_1	30 868	0.92	$6d^47s^27p$	$4^{\circ}_{1/2}$	35 408	2.22
(26) $6d^37s^27p$	4°_3	31 647	1.34	$6d^47s^27p$	$5^{\circ}_{3/2}$	35 447	1.00
(27) $6d^37s^27p$	6°_2	32 040	1.13	$6d^47s^27p$	$6^{\circ}_{5/2}$	35 774	1.34
(28) $6d^37s^27p$	3°_4	32 073	1.00	$6d^47s^27p$	$5^{\circ}_{7/2}$	36 251	1.00
(29) $6d^37s^27p$	4°_0	32 381	0.00	$6d^47s^27p$	$6^{\circ}_{3/2}$	36 333	1.02
(30) $6d^37s^27p$	6°_1	32 520	1.21	$6d^47s^27p$	$7^{\circ}_{5/2}$	36 875	1.25
(31) $6d^47s7p$	$^5D_3^{\circ}$	32 885	1.47	$6d^47s^27p$	$1^{\circ}_{11/2}$	37 542	1.10
(32) $6d^37s^27p$	4°_4	33 339	1.23	$6d^47s^27p$	$6^{\circ}_{7/2}$	37 910	1.32
(33) $6d^37s^27p$	7°_2	33 602	1.08	$6d^47s^27p$	$7^{\circ}_{3/2}$	37 954	1.05
(34) $6d^37s^27p$	8°_2	34 147	1.45	$6d^57s7p$	$8^{\circ}P_{9/2}^{\circ}$	37 972	1.62
(35) $6d^37s^27p$	2°_5	34 380	1.12	$6d^47s^27p$	$4^{\circ}_{9/2}$	38 336	1.23
(36) $6d^37s^27p$	6°_3	34 538	1.13	$6d^47s^27p$	$8^{\circ}_{5/2}$	39 454	1.19
(37) $6d^37s^27p$	7°_1	35 110	1.42	$6d^47s^27p$	$7^{\circ}_{7/2}$	39 602	1.33
(38) $6d^37s^27p$	7°_3	35 897	1.31	$6d^47s^27p$	$5^{\circ}_{1/2}$	40 273	1.76
(39) $6d^37s^27p$	5°_4	36 629	1.29				
(40) $6d^37s^27p$	9°_2	36 695	1.24				
(41) $6d^37s^27p$	8°_3	36 846	1.18				
(42) $6d^37s^27p$	8°_1	37 169	1.30				
(43) $6d^37s^27p$	6°_4	37 218	1.25				
(44) $6d^37s^27p$	3°_5	37 542	1.26				
(45) $6d^37s^27p$	5°_0	38 322	0.00				
(46) $6d^37s^27p$	9°_3	38 547	1.12				
(47) $6d^37s^27p$	10°_2	38 915	1.22				
(48) $6d^37s^27p$	7°_4	39 138	1.30				
(49) $6d^37s^27p$	4°_5	39 337	1.23				
(50) $6d^37s^27p$	10°_3	39 725	1.23				
(51) $6d^37s^27p$	9°_1	40 073	1.62				

Table IV. Low-lying spectrum of even and odd states parity for Hs I and Mt I. We present the energy and Landé g-factor for each state J^{parity} . We present LS - notations only for comparison with lighter analogs. For SHE states where an analogous state cannot be found in the lighter analog the term is labeled according to the sequential number of the state (n) for the given J^{parity} group, n_J^{parity} .

Hs I				Mt I			
Major Configuration	Term	Energy (cm ⁻¹)	Landé g-factor	Major Configuration	Term	Energy (cm ⁻¹)	Landé g-factor
Even parity states							
(1) $6d^67s^2$	5D_4	0	1.37	$6d^77s^2$	$^4F_{9/2}$	0	1.265
(2) $6d^67s^2$	5D_2	2 102	1.38	$6d^77s^2$	$^4F_{3/2}$	5 047	1.214
(3) $6d^67s^2$	5D_0	7 400	0.00	$6d^77s^2$	$^4F_{5/2}$	7 996	1.222
(4) $6d^67s^2$	5D_3	8 270	1.43	$6d^77s^2$	$^4F_{7/2}$	12 628	1.213
(5) $6d^67s^2$	5D_1	9 285	1.41	$6d^77s^2$	$^2G_{3/2}$	17 368	0.931
(6) $6d^67s^2$	3H_5	15 816	1.11	$6d^77s^2$	$^2G_{5/2}$	18 467	1.409
Odd parity states							
(7) $6d^57s^27p$	1°_2	13 093	1.98	$6d^67s^27p$	$1^{\circ}_{7/2}$	21 879	1.44
(8) $6d^57s^27p$	1°_3	15 600	1.58	$6d^67s^27p$	$1^{\circ}_{9/2}$	24 388	1.33
(9) $6d^57s^27p$	2°_2	23 708	1.30	$6d^67s^27p$	$1^{\circ}_{3/2}$	24 524	1.51
(10) $6d^57s^27p$	2°_3	26 492	1.16	$6d^67s^27p$	$1^{\circ}_{5/2}$	25 990	1.25
(11) $6d^67s7p$	$^7D_4^{\circ}$	27 394	1.58	$6d^67s^27p$	$2^{\circ}_{5/2}$	31 975	1.54
(12) $6d^57s^27p$	1°_1	29 444	1.17	$6d^67s^27p$	$1^{\circ}_{1/2}$	32 851	0.81
(13) $6d^57s^27p$	3°_2	29 794	1.34	$6d^77s7p$	$^6D_{9/2}^{\circ}$	33 505	1.40
(14) $6d^67s7p$	$^7D_5^{\circ}$	30 863	1.37	$6d^67s^27p$	$2^{\circ}_{1/2}$	34 665	1.51
(15) $6d^57s^27p$	3°_3	30 908	1.32	$6d^67s^27p$	$2^{\circ}_{7/2}$	35 117	1.29
(16) $6d^57s^27p$	4°_2	31 165	1.33	$6d^67s^27p$	$2^{\circ}_{3/2}$	36 159	1.13
(17) $6d^57s^27p$	2°_4	31 295	1.40	$6d^77s7p$	$^6F_{11/2}^{\circ}$	38 027	1.31
(18) $6d^57s^27p$	1°_0	31 552	0.00	$6d^67s^27p$	$3^{\circ}_{7/2}$	38 450	1.17
(19) $6d^57s^27p$	3°_4	32 522	1.26	$6d^67s^27p$	$3^{\circ}_{9/2}$	39 296	1.13
(20) $6d^57s^27p$	5°_2	33 694	1.44	$6d^67s^27p$	$2^{\circ}_{11/2}$	41 310	1.33
(21) $6d^57s^27p$	4°_3	33 920	1.03				
(22) $6d^57s^27p$	2°_1	34 076	1.52				
(23) $6d^57s^27p$	2°_5	34 739	1.20				
(24) $6d^57s^27p$	5°_3	34 812	1.41				
(25) $6d^57s^27p$	4°_4	35 689	1.23				
(26) $6d^67s7p$	$^7D_3^{\circ}$	35 705	1.56				
(27) $6d^57s^27p$	3°_1	35 990	1.81				
(28) $6d^67s7p$	$^7D_2^{\circ}$	37 036	1.40				
(29) $6d^67s7p$	$^7P_3^{\circ}$	37 237	1.33				
(30) $6d^57s^27p$	5°_4	37 443	1.18				
(31) $6d^57s^27p$	7°_2	38 519	1.34				
(32) $6d^67s7p$	$^7P_4^{\circ}$	39 025	1.29				
(33) $6d^57s^27p$	3°_5	39 268	1.27				
(34) $6d^67s7p$	$^7D_1^{\circ}$	39 512	2.11				
(35) $6d^57s^27p$	8°_3	39 652	1.38				
(36) $6d^57s^27p$	9°_3	40 783	1.19				

Table V. Strong electric dipole transitions and isotopic shift parameters for Sg I, Bh I, Hs I and Mt I. Only direct optical transitions to the ground state satisfying the E1 transition selection rules are shown. Here D_{E1} is the transition amplitude in a.u., A_{E1} is the transition rate, a , F , and \tilde{F} are calculated isotopic shift parameters for the charge radius discussed in Section IV. The numbers in parentheses correspond to the numbered states in Tables III and IV for the respective element.

State	D_{E1} (a.u)	A_{E1} ($\times 10^6$ s $^{-1}$)(cm $^{-1}$)	a (cm $^{-1}$)	F ($\frac{\text{cm}^{-1}}{\text{fm}^2}$)	\tilde{F} (cm $^{-1}$)	State	D_{E1} (a.u)	A_{E1} ($\times 10^6$ s $^{-1}$)(cm $^{-1}$)	a (cm $^{-1}$)	F ($\frac{\text{cm}^{-1}}{\text{fm}^2}$)	\tilde{F} (cm $^{-1}$)
Sg I (Ground state: 5D_0)						Bh I (Ground State: $^6S_{5/2}$)					
(8) 1°_1	0.639	1.36	9.41	2.04	11.9	(9) $^6D_{3/2}^{\circ}$	-0.172	0.107	18.1	3.74	22.8
(12) 2°_1	-0.160	0.192	-2.95	-0.639	-3.73	(10) $^8P_{5/2}^{\circ}$	-0.474	0.812	83.4	17.2	105
(14) 3°_1	1.17	13.4	4.90	1.06	6.18	(11) $^6P_{3/2}^{\circ}$	-0.494	1.38	-101	-20.7	-127
(19) $^3P^{\circ}_1$	-0.163	0.353	-19.7	-4.25	-24.8	(12) $^6D_{5/2}^{\circ}$	-0.0391	0.00611	-120	-24.6	-151
(25) 5°_1	0.592	6.97	6.58	1.42	8.30	(13) $^8P_{7/2}^{\circ}$	0.500	0.858	84.5	17.4	107
(30) 6°_1	-0.412	3.95	7.01	1.52	8.85	(14) $^6D_{7/2}^{\circ}$	0.345	0.471	-63.3	-13.0	-79.7
(37) 7°_1	-0.302	2.67	1.66	0.36	2.10	(16) $^6F_{5/2}^{\circ}$	1.51	16.6	-160	-33.0	-202
(42) 8°_1	0.148	0.761	3.55	0.768	4.48	(18) $^3\textcircled{3}_{3/2}$	1.50	30.0	-64.9	-13.4	-81.7
(51) 9°_1	0.524	11.9	-4.77	-1.03	-6.01	(19) $^3\textcircled{7}_{7/2}$	1.75	23.3	44.0	9.06	55.4
						(20) $^4\textcircled{5}_{5/2}$	-0.433	1.90	-101	-20.7	-127
						(21) $^4\textcircled{7}_{7/2}$	1.88	31.2	-380	-78.4	-479
						(22) $^4\textcircled{3}_{3/2}$	-0.998	18.6	-41.3	-8.51	-52
						(24) $^5\textcircled{5}_{5/2}$	-0.101	0.131	-105	-21.6	-132
						(26) $^5\textcircled{3}_{3/2}$	0.438	4.27	-135	-27.9	-170
						(27) $^6\textcircled{5}_{5/2}$	-1.06	17.1	-364	-74.9	-458
						(28) $^5\textcircled{7}_{7/2}$	0.0665	0.0361	-34.7	-7.15	-43.7
						(29) $^6\textcircled{3}_{3/2}$	0.160	0.615	-70.6	-14.5	-88.9
						(30) $^7\textcircled{5}_{5/2}$	-0.539	4.86	-335	-69.0	-422
						(33) $^6\textcircled{7}_{7/2}$	-0.674	6.18	-129	-26.6	-163
						(34) $^7\textcircled{3}_{3/2}$	0.387	4.09	-513	-106	-647
						(37) $^8\textcircled{5}_{5/2}$	0.232	1.10	-561	-116	-707
						(38) $^7\textcircled{7}_{7/2}$	0.516	4.13	-364	-75.1	-459
Hs I (Ground State: 5D_4)						Mt I (Ground State: $^4F_{9/2}$)					
(8) 1°_3	0.501	0.276	22.7	4.45	28.9	(7) $1^{\circ}_{7/2}$	0.0537	0.00765	27.5	5.10	34.5
(10) 2°_3	0.224	0.269	22.9	4.49	28.8	(8) $1^{\circ}_{9/2}$	0.432	0.550	27.6	5.13	34.7
(11) $^7D^{\circ}_4$	-1.11	5.66	-29.1	-5.70	-36.6	(13) $^6D^{\circ}_{9/2}$	1.27	12.3	-51.7	-9.60	-64.9
(14) $^7D^{\circ}_5$	0.999	5.41	-26.2	-5.15	-33.0	(15) $2^{\circ}_{7/2}$	-0.294	0.946	33.3	6.18	41.8
(15) 3°_3	0.208	0.370	16.2	3.18	20.4	(17) $^6F^{\circ}_{11/2}$	-1.89	33.3	-47.9	-8.89	-60.1
(17) 2°_4	0.0934	0.0603	5.54	1.09	6.98	(19) $^3\textcircled{9}_{9/2}$	0.0954	0.112	19.0	3.53	23.9
(19) 3°_4	0.120	0.112	18.5	3.62	23.2	(20) $2^{\circ}_{11/2}$	0.170	0.344	25.7	4.78	32.3
(21) 4°_3	-0.150	0.253	20.7	4.05	26.0						
(23) 2°_5	-1.13	9.88	12.3	2.42	15.5						
(24) 5°_3	1.70	35.5	12.3	2.41	15.5						
(25) 4°_4	0.798	6.52	7.84	1.54	9.87						
(26) $^7D^{\circ}_3$	-0.493	3.20	-33.3	-6.53	-41.9						
(29) $^7P^{\circ}_3$	-0.511	3.91	-15.8	-3.11	-19.9						
(30) 5°_4	-0.297	1.04	1.95	0.382	2.45						
(32) $^7P^{\circ}_4$	0.425	2.41	-9.56	-1.87	-12.0						
(33) 3°_5	2.64	77.5	5.16	1.01	6.49						
(35) 7°_3	2.10	80.0	-2.30	-0.451	-2.89						

Table VI. Theoretical and experimental ionization potentials of open $5d$ -shell elements. The CIPT energies are the results of the present work.

Atom	Ionic State	J	IP (eV)		
			Expt. [37]	CIPT	MCDF
Ta	$5d^36s$	1	7.549	7.57	
W	$5d^46s$	1/2	7.864	7.90	6.97 [65]
Re	$5d^56s$	3	7.833	7.85	6.84 [66]
Os	$5d^66s$	9/2	8.438	8.69	7.45 [66]
Ir	$5d^76s$	5	8.967	9.27	

Table VII. Some excitation energies (cm^{-1}) in open $6d$ -shell SHE and their lighter analogs. The CIPT energies are the results of the present work.

Atom	State	Expt. [37]	CIPT	MCDF [65, 66]
W	$5d^46s^2$ 5D_1	1670	1502	1162
	5D_2	3325	2664	2581
Re	$5d^56s6p$ $^8P_{5/2}^o$	18950		14000
Os	$5d^66s6p$ $^7D_3^o$	23463	26000	20500
Sg	$6d^47s^2$ 5D_1		4834	4186
	5D_2		7614	7211
Bh	$6d^57s7p$ $^8P_{5/2}^o$		2220	15100
Hs	$6d^57s^27p$ $^5S_2^o$		13100	5100
	$^5D_3^o$		15600	8600

Table VIII. Ionization potentials of open $6d$ -shell SHE, including ions. The CIPT energies are the results of the present work.

Atom or ion	Ground State	J	IP (eV)			
			CIPT	RHF ^a	MCDF [65, 66]	Extrap. [65, 66]
Db I	$6d^37s^2$	2	7.01	6.75		
Sg I	$6d^47s^2$	0	8.22	7.70	7.03	7.85
Sg II	$6d^37s^2$	3/2	18.0		15.85	17.06
Sg III	$6d^27s^2$	2	24.8		24.61	25.74
Bh I	$6d^57s^2$	5/2	8.03	8.63	6.82	7.7
Bh II	$6d^47s^2$	0	19.0		16.55	17.5
Bh III	$6d^47s$	1/2	26.2		25.64	26.6
Bh IV	$6d^4$	0	36.8		36.33	37.3
Hs I	$6d^67s^2$	4	8.52	9.52	6.69	7.6
Hs II	$6d^57s^2$	5/2	19.7		16.62	18.2
Hs III	$6d^47s^2$	3	27.7		27.12	29.3
Hs IV	$6d^47s$	1/2	40.5		36.59	37.7
Hs V	$6d^4$	0	50.6		50.37	51.2
Mt I	$6d^77s^2$	9/2	9.86	10.4		
Mt II	$6d^67s^2$	4	20.7			
Mt III	$6d^57s^2$	5/2	28.4			
Mt IV	$6d^57s$	3	43.3			
Mt V	$6d^5$	5/2	50.3			

^a Relativistic Hartree-Fock with semi-empirical core polarisation correction [20]